Cell Stem Cell
Article

Nodal/Activin Signaling Drives Self-Renewal and Tumorigenicity of Pancreatic Cancer Stem Cells and Provides a Target for Combined Drug Therapy

Enza Lonardo,[1] Patrick C. Hermann,[1] Maria-Theresa Mueller,[4] Stephan Huber,[5] Anamaria Balic,[1] Irene Miranda-Lorenzo,[1] Sladjana Zagorac,[1] Sonia Alcala,[1] Iker Rodriguez-Arabaolaza,[1] Juan Carlos Ramirez,[8] Raul Torres-Ruíz,[8] Elena Garcia,[2] Manuel Hidalgo,[2] David Álvaro Cebrián,[3] Rainer Heuchel,[9] Matthias Löhr,[9] Frank Berger,[6] Peter Bartenstein,[7] Alexandra Aicher,[1] and Christopher Heeschen[1,*]
[1]Clinical Research Programme, Stem Cells and Cancer Group
[2]Gastrointestinal Cancer Clinical Research Unit
[3]Experimental Therapeutics Programme
Spanish National Cancer Research Centre (CNIO), Madrid 28029, Spain
[4]Department of Surgery, Ruprecht Karl University, Heidelberg 69120, Germany
[5]Department of Surgery
[6]Department of Radiology
[7]Department of Nuclear Medicine
Ludwig-Maximilian-University, Munich 81377, Germany
[8]Viral Vector Unit, Spanish National Cardiovascular Research Centre (CNIC), Madrid, Spain
[9]Karolinska Institutet, Solna 171 65, Sweden
*Correspondence: christopher.heeschen@cnio.es
DOI 10.1016/j.stem.2011.10.001

SUMMARY

Nodal and Activin belong to the TGF-β superfamily and are important regulators of embryonic stem cell fate. Here we investigated whether Nodal and Activin regulate self-renewal of pancreatic cancer stem cells. Nodal and Activin were hardly detectable in more differentiated pancreatic cancer cells, while cancer stem cells and stroma-derived pancreatic stellate cells markedly overexpressed Nodal and Activin, but not TGF-β. Knockdown or pharmacological inhibition of the Nodal/Activin receptor Alk4/7 in cancer stem cells virtually abrogated their self-renewal capacity and in vivo tumorigenicity, and reversed the resistance of orthotopically engrafted cancer stem cells to gemcitabine. However, engrafted primary human pancreatic cancer tissue with a substantial stroma showed no response due to limited drug delivery. The addition of a stroma-targeting hedgehog pathway inhibitor enhanced delivery of the Nodal/Activin inhibitor and translated into long-term, progression-free survival. Therefore, inhibition of the Alk4/7 pathway, if combined with hedgehog pathway inhibition and gemcitabine, provides a therapeutic strategy for targeting cancer stem cells.

INTRODUCTION

Although pancreatic ductal adenocarcinoma has become the subject of increasing research efforts over the past decades, poor response to therapy with subsequent dismal survival has remained the hallmark of this disease. Recent evidence from our and other laboratories suggests that pancreatic carcinomas harbor a distinct subpopulation of putative cancer stem cells (CSCs) defined by their self-renewal capacity, differentiation ability, exclusive in vivo tumorigenicity (Hermann et al., 2007; Li et al., 2007), and ability to drive metastasis (Hermann et al., 2008). Most importantly, CSCs have also been proposed as the major source of resistance toward conventional chemotherapy and radiotherapy (Bar et al., 2007; Hermann et al., 2007; Mueller et al., 2009). Therefore, novel therapies capable of eliminating CSCs while leaving normal stem cells unaffected are urgently needed.

Members of the TGF-β family, namely Bone Morphogenic Proteins (BMPs), TGF-β, and Nodal/Activin, exert multiple, and sometimes opposing, effects on a variety of cell types depending on the cellular context, including the stage of the disease, the local environment, and the identity and the dosage of the ligand (Massagué, 2008; Watabe and Miyazono, 2009). Nodal and Activin as secreted proteins are expressed during embryonic development and are implicated in developmental events such as mesoderm formation and left-right axis specification. Moreover, they were shown to be essential for human embryonic stem cell (ESC) maintenance (Vallier et al., 2005; Xiao et al., 2006), but their role in cancer still remains poorly defined. Nodal and Activin bind to their common receptors, the *A*ctivin-*like* (Alk) type I receptors Alk4 and 7, while Cripto-1 constitutes an important coreceptor for Nodal signaling only (Strizzi et al., 2005). Recently, Nodal signaling was linked to a more aggressive phenotype in melanoma and breast cancer cells (Topczewska et al., 2006). Furthermore, inhibition of Nodal signaling has been shown to reduce tumorigenicity in melanoma cell lines, suggesting a potential role in tumor-initiating cells (Postovit et al., 2008). Encouraged by these reports, we investigated the role of the Nodal/Activin signaling cascade in the tumorigenic stem cell compartment of

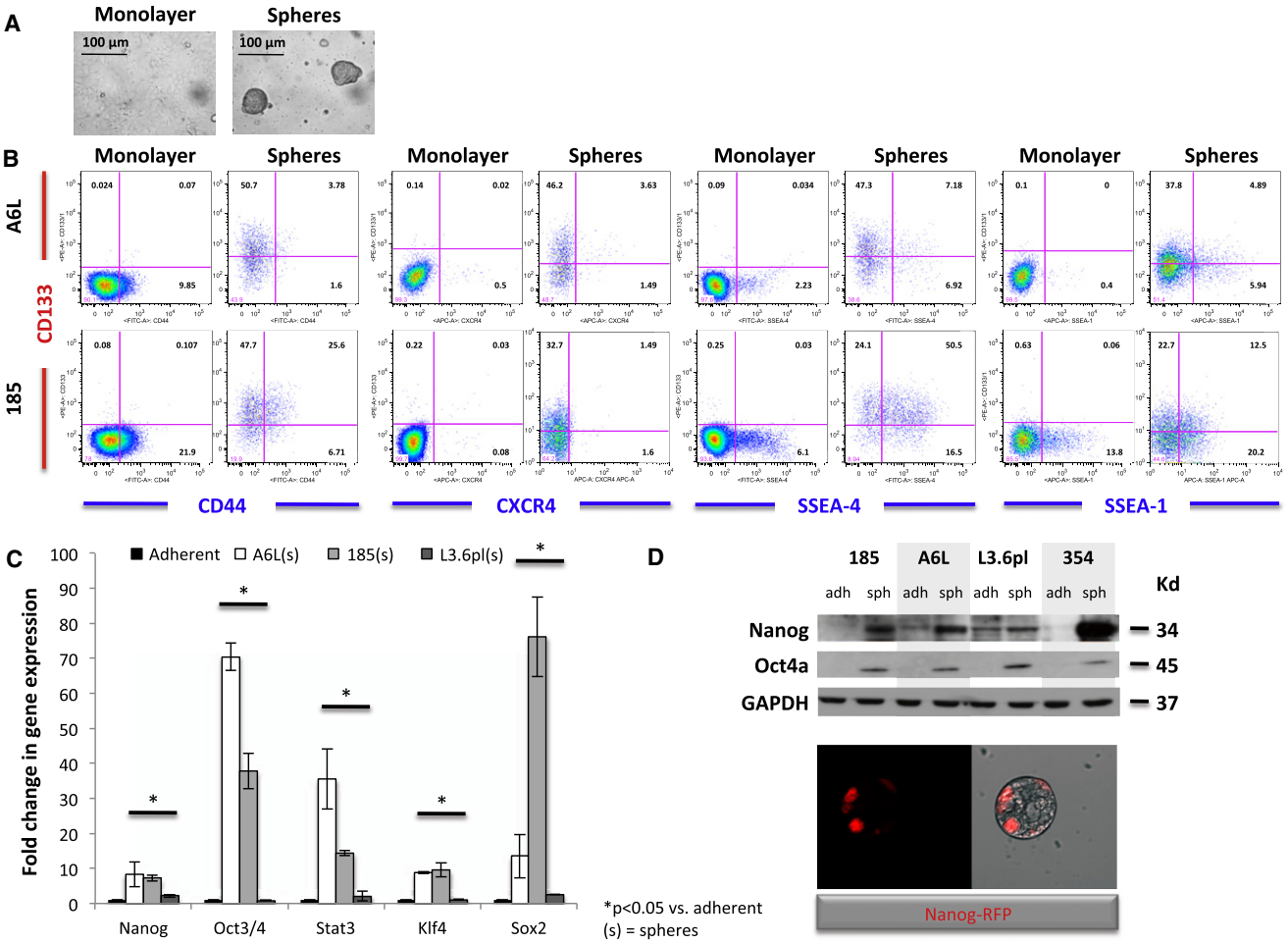

Figure 1. Sphere-Derived Pancreatic CSCs Express Pluripotency Markers

(A) Morphology of pancreatic cancer cells derived from xenografts and freshly isolated human tissue grown as monolayers or spheres.

(B) Flow cytometry analysis for CD44, CD133, CXCR4, SSEA-4, and SSEA-1 as cancer stem cell markers in spheres as compared with adherent cells from A6L or 185 tumors.

(C) qPCR analysis of pluripotency-associated genes in adherent cells versus spheres. Data are normalized to GAPDH expression and are presented as fold change in gene expression relative to adherent cells.

(D) Western blot analysis of Nanog, Oct4a, and GAPDH in spheres as compared with adherent cells. Nanog promoter RFP reporter construct illustrates the presence of single Nanog promoter^{+} cells in spheres.

pancreatic cancer, and its potential as a therapeutic target for the successful elimination of pancreatic CSCs as the root of this deadly disease.

RESULTS

Pancreatic CSCs Express Pluripotency-Associated Markers

We have shown that primary pancreatic CSCs can be enriched in vitro as anchorage-independent spherical colonies termed spheres (Hermann et al., 2007). These spheres are composed of a small number of cells with stem cell-like properties including the ability to form secondary spheres as well as more differentiated progenies. Recently, we also reported the enrichment of pancreatic CSCs within the CD133^{+}-expressing cell population as assessed by flow cytometry (Hermann et al., 2007). Therefore, for the present studies, we used these two supplementary methods for studying pancreatic CSCs.

A total number of eight human pancreatic adenocarcinoma xenografts were used, with A6L, 185, JH051, 247, and 198 being described earlier as primary tumors or tumor-derived primary cell lines (Jones et al., 2008; Rubio-Viqueira et al., 2006), and with 265, 286, and 354 produced by the same technique. Importantly, all cells for in vitro experiments were freshly isolated from early passage xenografts. Isolated cells from these xenografts were cultured as adherent cells (monolayer) or anchorage-independent spheres at low passages (Figure 1A). Moreover, three established pancreatic cancer cell lines (L3.6pl, MiaPaCa2, and Panc1) were used. Cells were phenotyped by flow cytometry for the expression of CD133, CD44, CXCR4, SSEA-4, and SSEA-1. As previously reported, spheres are enriched in CD133^{+} cells, as well as several other markers that have been associated with a CSC phenotype such as CXCR4, SSEA-4, and SSEA-1, as

compared with adherent cells (Hermann et al., 2007; Scaffidi and Misteli, 2011). In contrast, cells expressing adhesion molecules such as CD44 (Figure 1B) and EpCAM (data not shown) were not consistently enriched in sphere culture, mostly likely reflecting anchorage-independent culture conditions, and were therefore not linked to a CSC phenotype in cultured cells (Figure S1A available online).

Next, the expression of pluripotency-associated genes (*Nanog*, *Oct3/4*, *Stat3*, *Klf4*, and *Sox2*) was determined by real-time PCR. Expression of pluripotency-associated genes was significantly higher in first generation sphere culture (d7) versus 70% confluent monolayer culture (Figure 1C). Intriguingly, the expression levels observed for pancreatic spheres were comparable to those of human ESCs (data not shown). Expression of protein levels was validated for Oct4a and Nanog by western blotting and using a Nanog promoter reporter construct (Figure 1D).

Components of the Nodal/Activin Signaling Cascade Are Overexpressed in Primary Pancreatic CSCs

Because the Nodal/Activin pathway is reportedly inactive in adult tissue (Hendrix et al., 2007; Topczewska et al., 2006), we determined whether this pathway is reactivated in pancreatic cancer (stem) cells by assessing mRNA expression for its components, namely *Nodal*, *Cripto-1*, *FoxH1*, *Smad2*, *Smad4*, *Gdf1*, *Activin*, and *Alk4*. Real-time PCR demonstrated that Nodal/Activin signaling-related genes are significantly overexpressed in first-passage spheres as compared with those in adherent cells, although marked differences in mRNA expression between the various tumors can be noted (Figure 2A). Interestingly, the expression further and strongly increased in second-passage spheres (Figure 2B). Western blot analysis demonstrated that Nodal is consistently and strongly overexpressed in spheres as compared with adherent cells on the protein level (Figure 2C), and that Alk4$^+$ as well as Cripto$^+$ cells are also enriched in sphere culture as determined by flow cytometry (Figure S1B). In contrast, mRNA levels for *TGF-β1*, TGF-β type I receptor/*Alk5*, and *TGF-β type II* receptor did not differ between sphere-derived cells and adherent cells, while flow cytometry revealed even decreased numbers of Alk5$^+$ cells in spheres (Figures S1B and S1C).

Most importantly, spheres showed enhanced expression of all essential components of the Nodal pathway including phosphorylation of Smad2. This allows its association with Smad4 followed by subsequent translocation to the nucleus to regulate target gene expression, suggesting that the Nodal signaling pathway is operational (Figure 2C). Nodal was hardly detectable in adherent cells by immunohistochemistry, while sphere-derived cells displayed strong cytoplasmic and membranous Nodal protein expression (Figure 2D). Data in established pancreatic cancer cell lines also showed increased expression of Nodal and some of its pathway components in sphere-derived cells, although differences were less pronounced as compared with primary cells, with no difference for the TGF-β signaling pathway (Figures S1D and S1E). We next validated our sphere-based in vitro data using magnetic activated cell sorting (MACS) of CD133$^+$ cells from freshly digested human pancreatic tumor xenografts (185, 198, and 354). Flow cytometry showed good depletion for CD133$^+$ cells in the CD133$^-$ population and revealed enrichment to ~75% in the CD133$^+$ population (Figure 2E). Real-time PCR analysis showed increased expression of Nodal-signaling-associated genes. Specifically, *Nodal*, *Cripto-1*, *Cripto-3*, *Activin*, and *Alk4* were overexpressed in CD133$^+$ cells as compared with CD133$^-$ cells (Figure 2F). Importantly, Nodal expression at the mRNA and protein level was not detectable in normal pancreatic tissue (Figure 2G), but Nodal was highly expressed in pancreatic cancer tissue with strong upregulation during development and progression of primary pancreatic ductal adenocarcinoma as shown in representative tissue microarray samples (Figures 2G and 2H). Because Nodal expression has recently been shown to be reactivated in breast cancer tissue (Topczewska et al., 2006), we also investigated the modulation of Nodal and its pathway components in putative MCF7 breast cancer stem cells (Engelmann et al., 2008). Consistent with the data obtained for pancreatic cancer cells, Nodal, its cofactor Cripto-1, and several pluripotency-associated markers were overexpressed in MCF7-derived spheres as compared with adherent cultures (Figures S1F and S1G). These results indicate that enhanced Nodal expression in the CSC fraction is not restricted to pancreatic cancer.

Nodal/Activin Signaling Is Functionally Active in Pancreatic CSCs

Nodal and Activin are secreted proteins that exert their function by binding to and joining the cell surface receptors Alk4 and Alk7 to form a tertiary ligand-receptor complex that leads to the phosphorylation of Smad2 or Smad3 as intracellular effectors and the subsequent regulation of cell functions. To determine whether rNodal and rActivin, respectively, are capable of activating this signaling cascade, we starved human primary sphere-derived CSCs as illustrated in Figure 3A. Cells were then treated with recombinant protein in the presence or absence of the Alk4/7 inhibitor SB431542 or LY2157299 (specific inhibitor of Alk5). After 30 min of stimulation, phosphorylation of Smad2 and expression of *Nanog*, *Oct3/4*, *Klf4*, *Sox2*, and *Stat3* were determined. Putative cytotoxicity of the utilized inhibitors was excluded by exposure of the cells to the inhibitors for 24 hr followed by DAPI/Annexin V staining (Figure 3B). rNodal/rActivin strongly induced phosphorylation of Smad2, while pretreatment with SB431542 partially abrogated Smad2 phosphorylation after stimulation with rNodal (Figures 3C and 3D). In contrast, TGF-β1 did not induce phosphorylation of Smad2 in sphere-derived cells; nor did the Alk5 inhibitor LY2157299 result in a reduced Smad2 phosphorylation. These results suggest that only Nodal and Activin are capable of activating the Alk4/7 signaling cascade by Smad2 phosphorylation in pancreatic CSCs.

Nodal and Activin Drive Self-Renewal of Pancreatic CSCs

To characterize the biological effects of Nodal and Activin on human pancreatic CSCs, we first examined whether Nodal is capable of enhancing colony formation and self-renewal capacity of pancreatic CSCs. In the sphere formation assay, single cells in suspension were treated with rNodal, rActivin, rTGF-β1, rLefty (endogenous direct inhibitor of Nodal), the Alk4/7 inhibitor SB431542, the specific Alk5 inhibitor LY2157299, and TGF-β receptor II neutralizing antibodies. After 7 days, treatment with rNodal increased the number of spheres as compared with control cells (Figure 4A). In contrast,

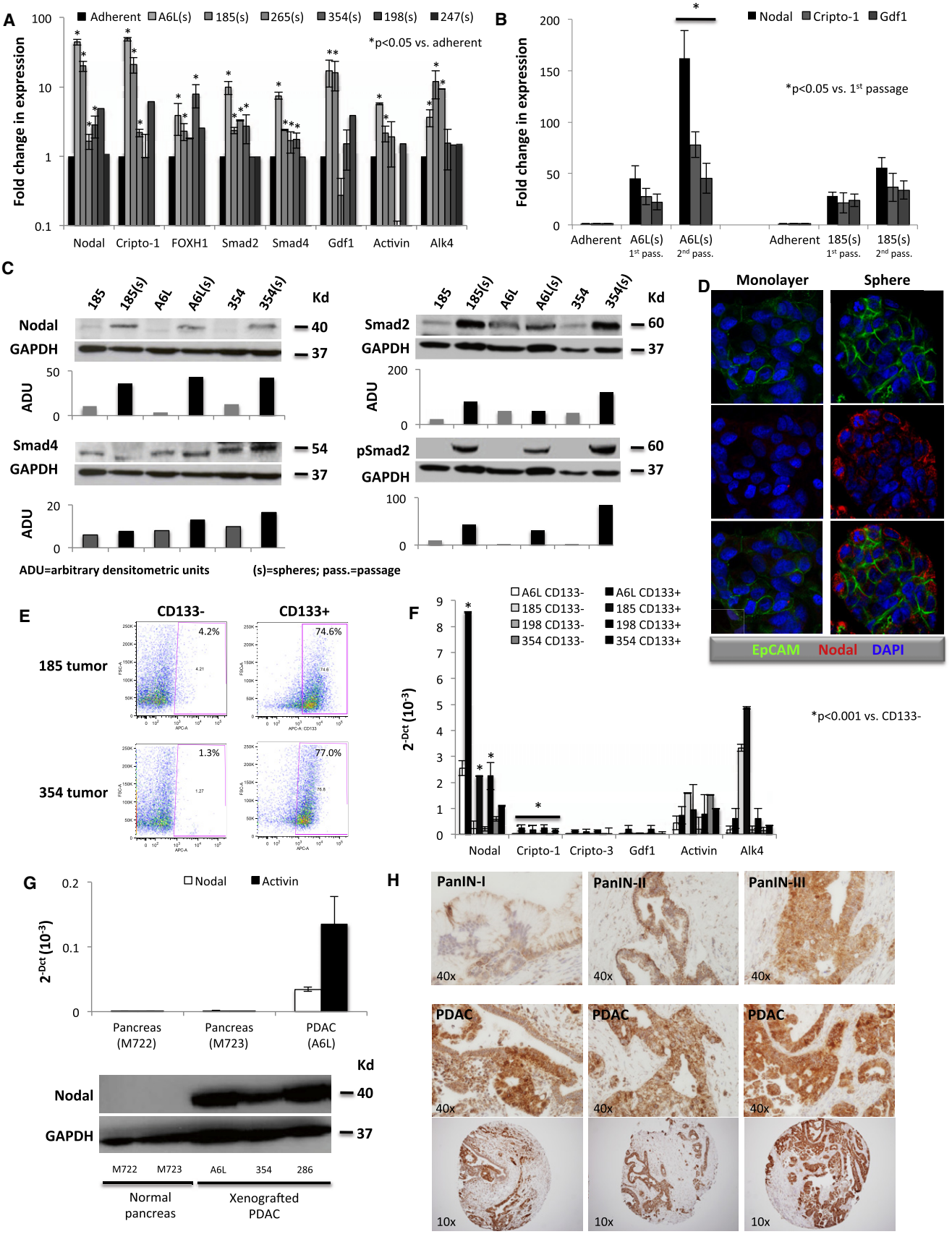
A
Adherent
A6L(s)
185(s)
265(s)
354(s)
198(s)
247(s)
*p<0.05 vs. adherent
Fold change in expression
Nodal
Cripto-1
FOXH1
Smad2
Smad4
Gdf1
Activin
Alk4
B
Nodal
Cripto-1
Gdf1
*p<0.05 vs. 1st passage
Fold change in expression
Adherent
A6L(s) 1st pass.
A6L(s) 2nd pass.
Adherent
185(s) 1st pass.
185(s) 2nd pass.
C
185
185(s)
A6L
A6L(s)
354
354(s)
Kd
Nodal
GAPDH
ADU
Smad4
Smad2
pSmad2
ADU=arbitrary densitometric units
(s)=spheres; pass.=passage
D
Monolayer
Sphere
EpCAM
Nodal
DAPI
E
CD133-
CD133+
185 tumor
354 tumor
4.2%
74.6%
1.3%
77.0%
F
A6L CD133-
185 CD133-
198 CD133-
354 CD133-
A6L CD133+
185 CD133+
198 CD133+
354 CD133+
2-Dct (10-3)
*p<0.001 vs. CD133-
Nodal
Cripto-1
Cripto-3
Gdf1
Activin
Alk4
G
Nodal
Activin
2-Dct (10-3)
Pancreas (M722)
Pancreas (M723)
PDAC (A6L)
Kd
Nodal
GAPDH
M722
M723
A6L
354
286
Normal pancreas
Xenografted PDAC
H
PanIN-I
PanIN-II
PanIN-III
PDAC
40x
10x

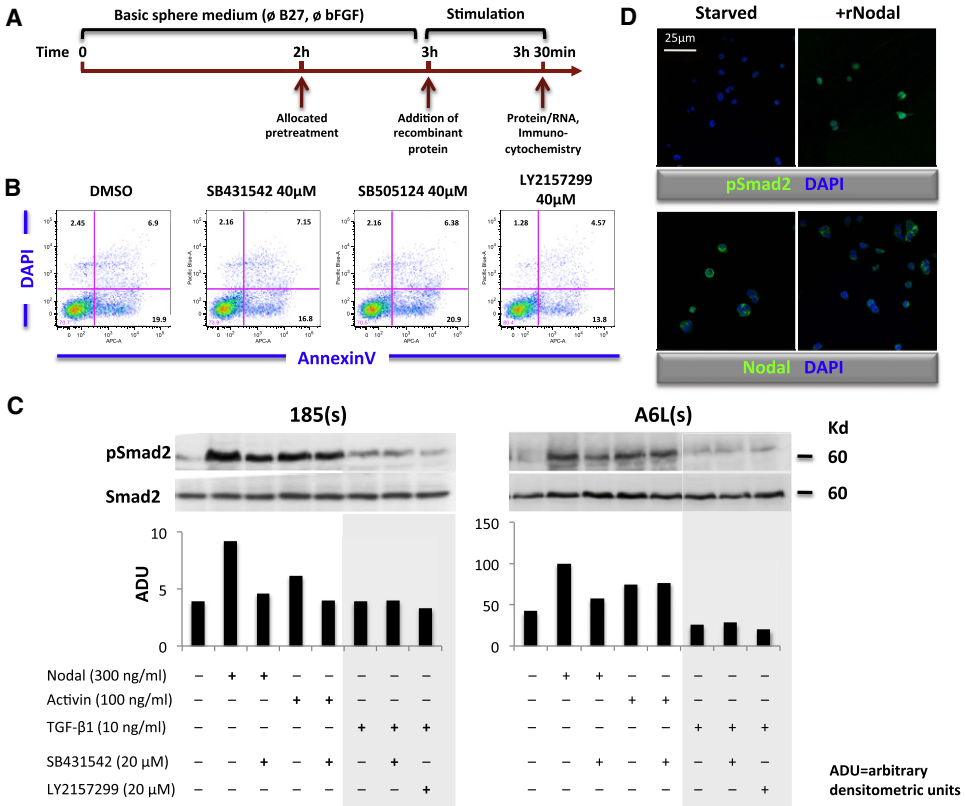

Figure 3. Nodal Signaling Is Functionally Active in Pancreatic CSCs

(A) Schematic illustration of Smad2 phosphorylation assay: cells were kept in basic sphere medium for 3 hr and stimulated for another 30 min with rNodal or rActivin alone or in combination with SB431542. After stimulation molecular and histological analyses were performed.

(B) Cell viability was determined by flow cytometry using DAPI/Annexin V.

(C) Western blotting for pSmad2 and Smad2 after stimulation with rNodal or rActivin alone or in combination with SB431542.

(D) Immunocytochemistry for pSmad2 and Nodal in A6L cells after stimulation with rNodal.

stimulation with rActivin did not result in a profound increase in sphere formation for all tested cells, but in long-term experiments, it did enhance the number of cells with active *Nanog* promoters in sphere cultures to the same extent as Nodal (Figure 4B). The diverse stimulatory effects of rNodal are most likely related to varying levels of endogenous Nodal expression in sphere-forming cells, because pretreatment with the Nodal-specific inhibitor rLefty or the less specific Alk4/7 inhibitor SB431542 dose-dependently (10, 20, and 40 µM) blocked sphere formation, whereas this was not the case in untreated cells (Figure 4A). Consistently, rNodal treatment resulted in the formation of more and larger colonies as compared with control, as determined by a soft agar assay (Figure S2). These data further corroborate the crucial importance of this pathway in the self-renewal capacity of pancreatic CSCs. In contrast, neither the Alk5 inhibitor LY2157299 nor TGF-β receptor II neutralizing antibodies resulted in significant changes in sphere-forming capacity (Figure 4A), suggesting that TGF-β signaling is not relevant for the self-renewal capacity of CSCs.

Next, we investigated the role of the TGF-β family members in the invasive capacity of pancreatic CSCs. A Matrigel-coated, modified Boyden chamber was used to quantitatively evaluate cell invasion. As shown in Figure 4C, the percentage of migrated cells increased significantly after stimulation with rNodal, rActivin, and TGF-β1. Inhibition of Alk4/7 by SB431542 as well as inhibition of Alk5 by SB505124 or the more specific

Figure 2. Components of the Nodal/Activin Signaling Pathway Are Overexpressed in Pancreatic CSCs

qPCR analysis of Nodal-signaling-associated genes in adherent cells versus spheres (s) in first (A) and second passage (B). Data are normalized to GAPDH expression and presented as fold change in gene expression relative to adherent cells. (C) Western blot analysis for Nodal, Smad4, pSmad2, and Smad2 proteins in adherent cells versus spheres. Parallel GAPDH immunoblotting was performed and signal quantification was performed by densitometry. (D) Confocal images for EpCAM (green), Nodal (red), and nuclei (blue) of adherent cells and spheres. (E) CD133 MACS of fresh tumor-derived cancer cells. Purity was validated by flow cytometry using CD133/2. (F) qPCR analysis for Nodal-signaling-associated genes in $CD133^{+}$ cells versus $CD133^{-}$ cells. Data are normalized to GAPDH. (G) qPCR analysis for Nodal and Activin in normal pancreatic tissue from healthy donors (M722 and M723) and pancreatic ductal adenocarcinoma (PDAC). (H) Immunohistochemistry for Nodal (brown) in tissue sections from patients with PanIN-I to PanIN-III lesions and three different patients with PDAC. See also Figure S1.

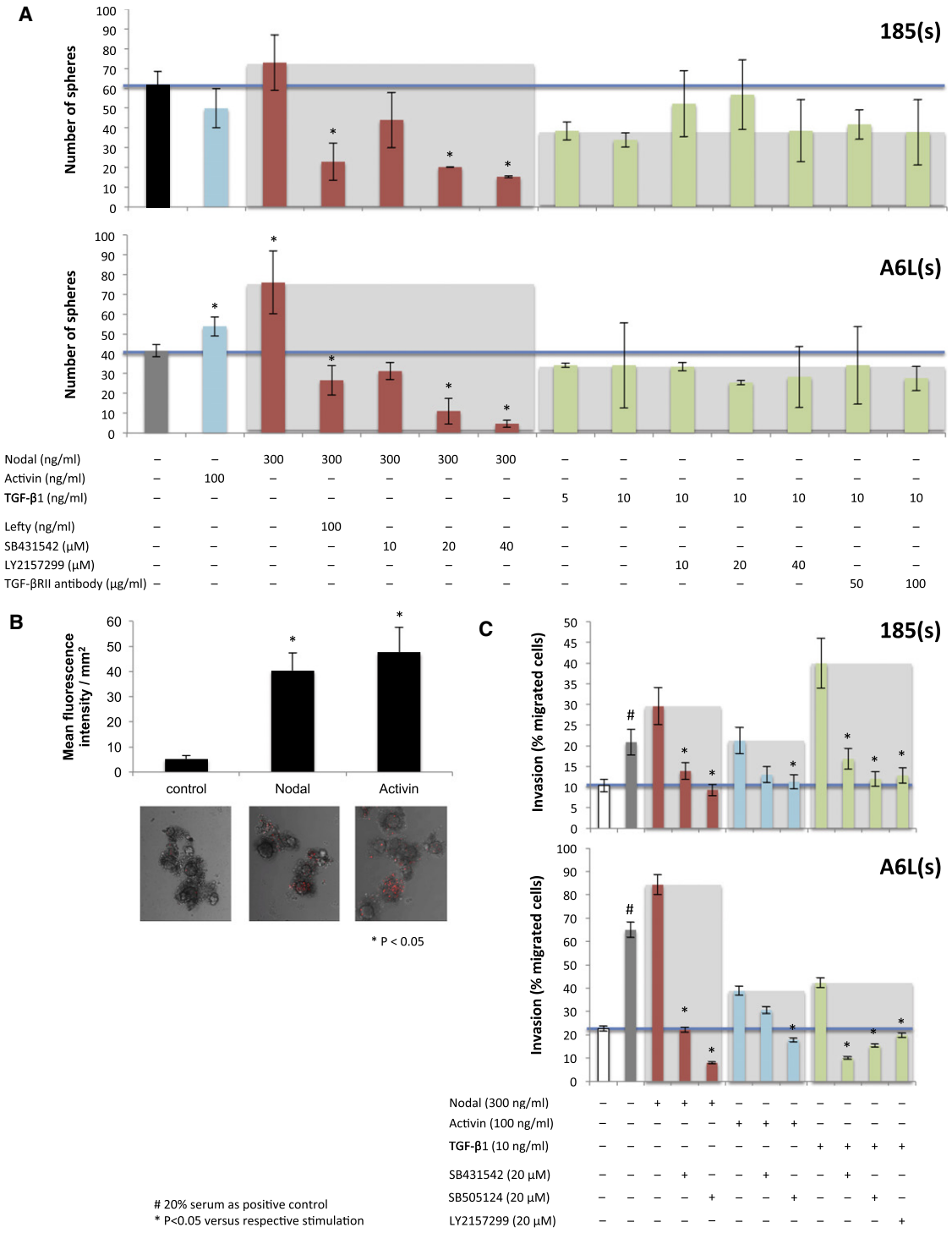

Figure 4. Pharmacological Inhibition of the Nodal/Activin or TGF-β Pathway

(A) Sphere formation capacity of 185 (top panel) and A6L (bottom panel) cells after treatment with the depicted combinations and concentrations of agonists and antagonists of the Nodal/Activin and TGF-β pathways.

(B) A *Nanog* reporter construct expressing RFP was used to detect Nanog promoter^{+} cells (red). Cells were treated with vehicle, rNodal, or rActivin.

(C) Invasion of sphere-derived 185 (top panel) and A6L (bottom panel) cells after treatment as depicted.

See also Figure S2.

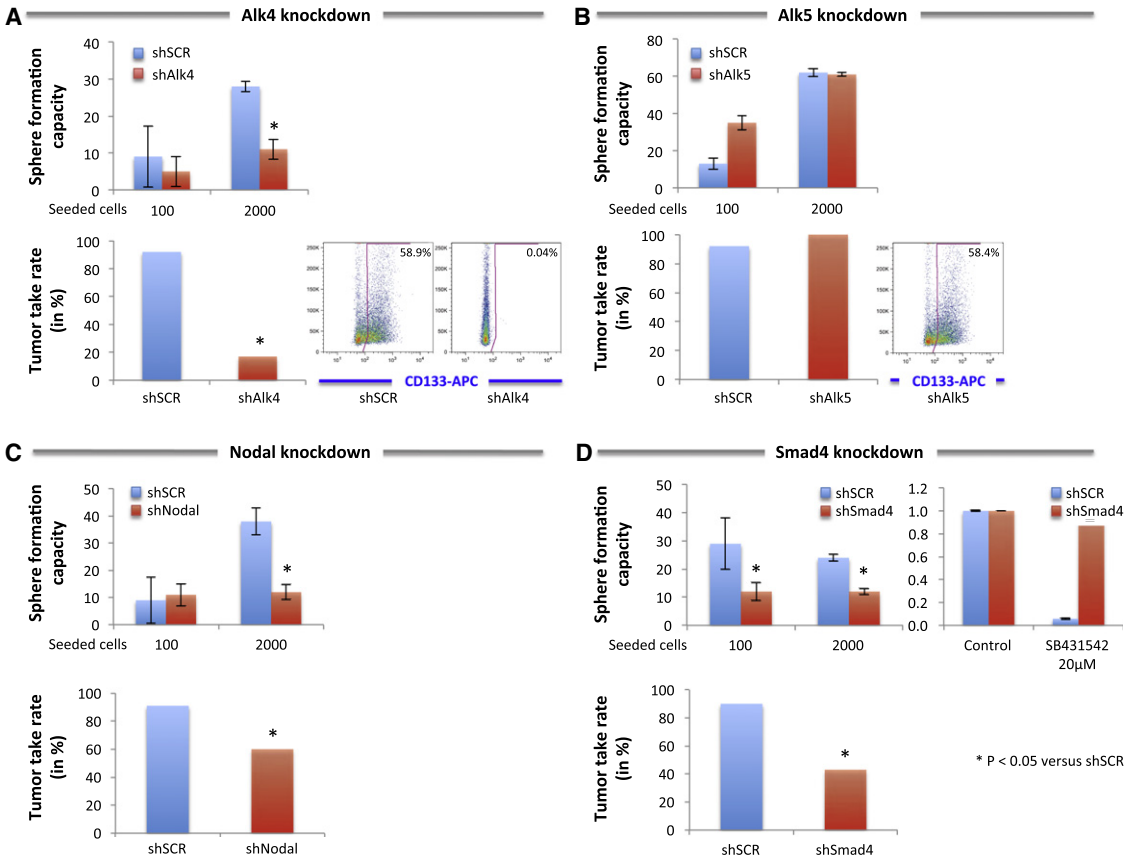

Figure 5. Genetic Targeting of the Nodal/Activin or TGF-β Pathway

(A) Lentivirally transduced cell cultures were sorted by FACS to highest purity based on GFP expression. Comparison of sphere formation capacity (upper panel), in vivo tumorigenicity (lower panel, left), and CD133 content of harvested tumors (lower panel, right) after lentiviral delivery of scrambled or *Alk4* shRNA is shown.

(B) As in (A), but with *Alk5* knockdown.

(C) Lentivirally transduced cell cultures were sorted by FACS to highest purity based on GFP expression. Comparison of sphere formation capacity (upper panel) and in vivo tumorigenicity (lower panel) after lentiviral delivery of scrambled or *Nodal* shRNA is shown.

(D) Lentivirally transduced cell cultures were selected using puromycin resistance. Comparison of sphere formation capacity (upper panel, left), response to SB431542 (upper panel, right), and in vivo tumorigenicity (lower panel) after lentiviral delivery of scrambled or *Smad4* shRNA is shown.

See also Figure S3.

compound LY2157299 completely blocked the enhanced invasiveness of pretreated CSCs. These data indicate that pancreatic CSCs are capable of responding to TGF-β1 by enhanced invasiveness, most likely via Smad2-independent mechanisms (Zhang, 2009).

Finally, the above findings were validated using specific genetic targeting of *Alk4*, *Alk5*, *Nodal*, and *Smad4* using lentiviral delivery of specific shRNA (Table S2 available online). Cells were either selected by FACS for GFP (Alk4, Alk5, Nodal) (Figures S3A–S3C) or by using puromycin resistance (Smad4) (Figure S3D). Knockdown of *Alk4*, which was validated by reduced surface expression of Alk4 as assessed by flow cytometry (Figure S3A), resulted in a significant reduction of sphere formation capacity and, most importantly, drastically reduced in vivo tumorigenicity (Figure 5A). In those few and diminutive tumors that actually formed, $CD133^+$ cells were undetectable. In contrast, knockdown of *Alk5*, also validated by reduced surface expression of Alk5 (Figure S3B), neither affected sphere formation capacity nor resulted in reduced in vivo tumorigenicity (Figure 5B). Consistently, the content of $CD133^+$ cells was not changed as compared with that of scrambled control. Importantly, population doubling of adherent cells was not significantly altered by either knockdown, indicating that these differences were not related to changes in proliferation rate (Figures S3A and S3B). Knockdown of *Nodal* also resulted in significantly lower sphere formation capacity (Figure 5C, Figure S3C). The strong knockdown of *Nodal* translated into significantly reduced in vivo tumorigenicity. Finally, knockdown of *Smad4*, a crucial component of the canonical Alk4/7 signaling cascade, led to a significant reduction in sphere formation capacity (Figure 5D, Figure S3D). Intriguingly, the *Smad4* knockdown translated into reduced in vivo tumorigenicity to a level that was comparable to inhibition of sphere formation and can be rationalized by downstream inhibition of the Nodal/Activin pathway. Indeed, while cells with scrambled shRNA strongly responded to SB431542, cells with knockdown for *Smad4* virtually lost

responsiveness to SB431542 with respect to sphere formation capacity (Figure 5D).

The observation that knockdown of *Nodal* resulted in a less pronounced reduction of in vivo tumorigenicity despite virtually complete knockdown of *Nodal* and strong inhibition of in vitro sphere formation suggests alternative sources for Nodal and/or Activin that may partially overcome the knockdown of *Nodal* in pancreatic CSCs in vivo. Indeed, we found robust expression of Nodal and Activin in human pancreatic stellate cells (PSCs) as an important stromal component of the pancreas (Jesnowski et al., 2005; Ohnishi et al., 2003) (Figure S4A). Sphere formation and invasion of pancreatic CSCs were significantly enhanced by PSC-conditioned medium, an effect that was abrogated by pretreatment with the Alk4/7 inhibitor SB431542 (Figures S4B and S4C). Together with the findings that knockdown of *Nodal* did translate into reduced sphere formation in vitro, but only moderately reduced tumorigenicity in vivo, while knockdown of *Alk4* resulted in strong reduction of both endpoints, we conclude that in vivo CSCs are most likely stimulated in both an autocrine and a paracrine fashion by the stromal compartment.

Nodal Inhibition Chemosensitizes Pancreatic CSCs to Chemotherapy

Pancreatic CSCs are inherently resistant to chemotherapy, resulting in relative enrichment for CSCs in adherent culture as evidenced by flow cytometry (Figure 6A) and an increase in Nodal expression (Figure 6B). Effects were more pronounced in CSC-enriched sphere cultures (Figure 6C). Intriguingly, using CD133 expression as readout for CSC content, we observed a virtually complete elimination of CSCs by inhibiting the Nodal/Activin pathway (Figure 6D), while population doubling was not affected (data not shown). This effect was most consistent in the presence of gemcitabine. These data were validated in freshly isolated patient-derived pancreatic cancer cells (Figure 6E).

For the subsequent investigation of in vivo tumorigenicity of pretreated cells as the most important endpoint, identical numbers of L3.6pl pancreatic cancer cells were exposed to gemcitabine alone, SB431542 alone, or both agents. All surviving cells were orthotopically implanted into the pancreas of immunocompromised mice. No further in vivo treatment was administered. Tumorigenicity was determined by noninvasive PET scan imaging on day 32 and macroscopic and microscopic evaluation on day 35. Importantly, only combination therapy was capable of eliminating in vivo tumorigenicity (Figures S5A–S5C). Mechanistically, we could show that despite a marked decrease in CD133 content following 4 days of treatment with SB431542 alone, the $CD133^+$ population replenished within 48 hr after withdrawal of treatment. When cells were treated with SB431542 and gemcitabine, however, the $CD133^+$ population was irreversibly eliminated (Figure S5D). To further elucidate the mechanism of this finding, we performed cell cycle analyses using BrdU. Treatment with SB431542 alone did not affect the percentage of $CD133^+$ cells in S phase, nor did it increase the percentage of apoptotic $CD133^+$ cells, while the addition of gemcitabine resulted in a 3-fold increase in apoptotic $CD133^+$ cells and virtually complete elimination of cells in S phase (Figure S5E). These findings indicate that SB431542 is capable of reversing the chemoresistance of the tumorigenic CSC population, most likely by (reversibly) driving them into a more differentiated state as evidenced by temporary loss of CD133.

Nodal/Activin Inhibition in Established Pancreatic Cancers

Based on these promising findings, we then investigated whether inhibition of Nodal/Activin by SB431542 translates into increased progression-free survival in pre-established pancreatic cancers. Because only the combination pretreatment with gemcitabine resulted in loss of tumorigenicity in vivo, we focused on this treatment regimen. Xenografts were established by orthotopic implantation of L3.6pl cells into athymic mice and treatment was started 1 week after injection. The detailed experimental setup is depicted in Figure 7A. Harvesting of some tumors after the last round of SB431542 administration revealed efficient in vivo targeting of the Nodal/Activin pathway with subsequent downregulation of Nodal (Figures S6A–S6D). Tumor growth was assessed on day 42 by palpation and confirmed by magnetic resonance imaging (MRI) (Figure 7B). No tumors were detectable in mice receiving combination therapy, so the study was continued until day 100 to monitor progression/putative relapse of disease. Over time, control animals bore large, life-limiting tumors and succumbed within 40 days after tumor implantation (median survival time: 32 days). Gemcitabine alone significantly prolonged survival due to inhibition of tumor growth, but all animals showed progressive disease with median survival still severely limited with 54 days. For the combination of SB431542 and gemcitabine, long-term survival was significantly better compared with gemcitabine alone, with 100% survival at day 100 (Figure 7C).

Next, we investigated the effects of SB431542 in primary human pancreatic cancer tissue xenografts as the ultimate preclinical setting (see study design in Figure 7D). In contrast to the above findings for implantation of cancer cells, the addition of SB431542 to gemcitabine treatment did not result in a deceleration of growth of primary tumor tissue (Figure 7E). During long-term follow-up, it was only when gemcitabine was already withdrawn that tumor growth eventually started to slow down, as compared with tumors treated with gemcitabine alone, while the latter actually reaccelerated in growth. This difference in response to gemcitabine withdrawal resulted in a modest, but significantly reduced, tumor burden at the 100 day follow-up point.

Based on this rather disappointing outcome and stimulated by data from Olive et al. (2009), we hypothesized that this modest treatment effect could be attributed to poor drug delivery in stroma-rich primary pancreatic cancer tissue. Indeed, mass spectrometry analysis revealed that SB431542 was hardly detectable in tumor-bearing mice after 2 weeks of treatment (Figure S6E). Intriguingly, the addition of the Smoothened inhibitor CUR199691 (CUR) for targeting the hedgehog pathway in stromal cells drastically improved drug delivery by 10-fold. Therefore, we next tested a triple combination therapy (gemcitabine, SB431542, and CUR), which translated into immediate inhibition of tumor progression and eventually translated into long-term stable disease at 100-day follow-up (Figures 7E and 7F and Figure S7A). Histological evaluation of the tumors explanted by the end of the study confirmed a marked depletion of tumor stroma in the triple therapy group, as well as a higher grade of differentiation, although the later changes were of a more subtle nature (Figure 7F). Cells isolated from harvested

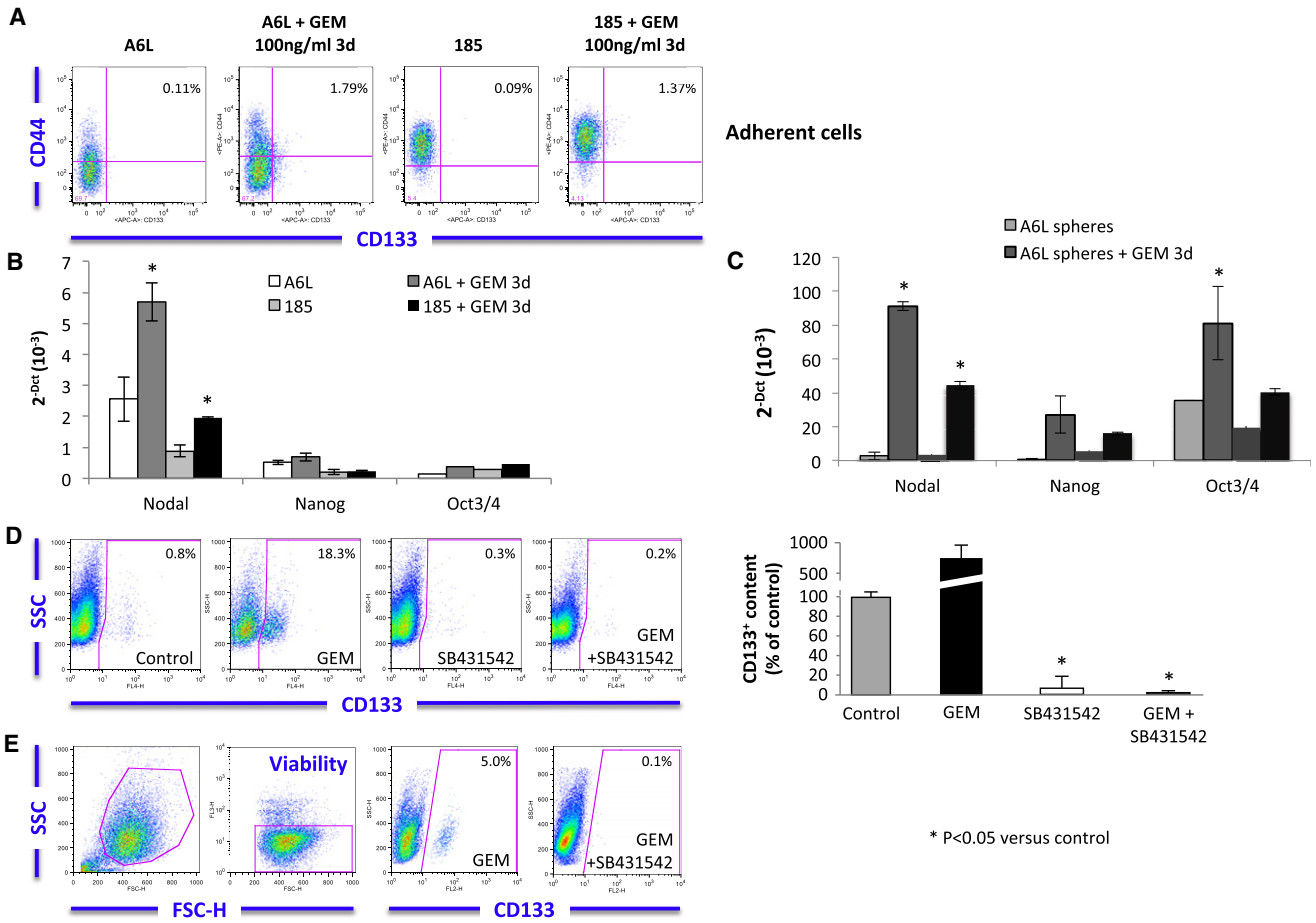

Figure 6. Nodal Inhibition Targets CD133$^+$ CSCs

(A) Flow cytometry for CD44 and CD133 in A6L and 185 adherent cells untreated or treated with gemcitabine (GEM). qPCR analysis for *Nodal*, *Nanog*, and *Oct3/4* genes in A6L and 185 adherent cells (B) or spheres (C) untreated or treated with GEM is shown. Data are normalized for GAPDH expression. (D) Flow cytometry for CD133 expression in L3.6pl cells untreated or treated as indicated (left panel). Quantification of CD133 expression in respective groups, with n = 3 (right panel), is shown; data are mean ± SEM, n ≥ 3. (E) Flow cytometry for CD133 in freshly isolated primary human pancreatic cancer cells treated with GEM in the presence or absence of SB431542. See also Figure S4.

tumors treated only with gemcitabine demonstrated strong sphere-forming capacity as opposed to cells isolated from tumors treated with gemcitabine plus SB431542, which already showed a significant reduction in sphere-forming capacity (Figure 7G, left panel). Most intriguingly, however, cells derived from tumors treated with triple therapy had virtually lost their sphere-forming capacity. Consistent patterns were observed for phenotyping of the cells using flow cytometry. CD133$^+$ or CD133$^+$/CD44$^+$ cells were significantly reduced in the group receiving triple combination therapy (Figure 7G, right panel). Consistently, administration of triple therapy to another tumor (JH051) resulted in similar treatment response. Taken together, these data demonstrate that triple therapy is capable of eliminating tumor-promoting pancreatic CSCs in vivo, leading to long-term progression-free survival.

DISCUSSION

Patients with pancreatic ductal adenocarcinoma are still suffering from a devastating prognosis, which can be at least partially rationalized by the observation that the standard chemotherapeutic agent gemcitabine is not capable of eliminating CSCs. Indeed, gemcitabine rather leads to a relative increase in the number of CSCs, indicating a preferential targeting of more differentiated and rapidly proliferating cancer cells. The restricted elimination of the more differentiated cancer cells, even if associated with significant tumor size reduction, will not lead to the eradication of the tumorigenic potential of the tumor, as that is restricted to the CSC population. Here we demonstrate that the Nodal/Activin pathway is essential for the self-renewal capacity and stemness properties of pancreatic CSCs. Nodal/Activin is strongly expressed in pancreatic CSCs, but is also expressed by PSCs, which are abundantly present in the stroma surrounding pancreatic cancer cells and may serve as a CSC niche.

In a large set of primary cells and (fresh) primary patient tissues, we then showed that the CSC compartment is severely affected by inhibition of this pathway by making use of three different approaches: first, by using a small molecule inhibitor (SB431542) targeting the Nodal/Activin receptor Alk4; second,

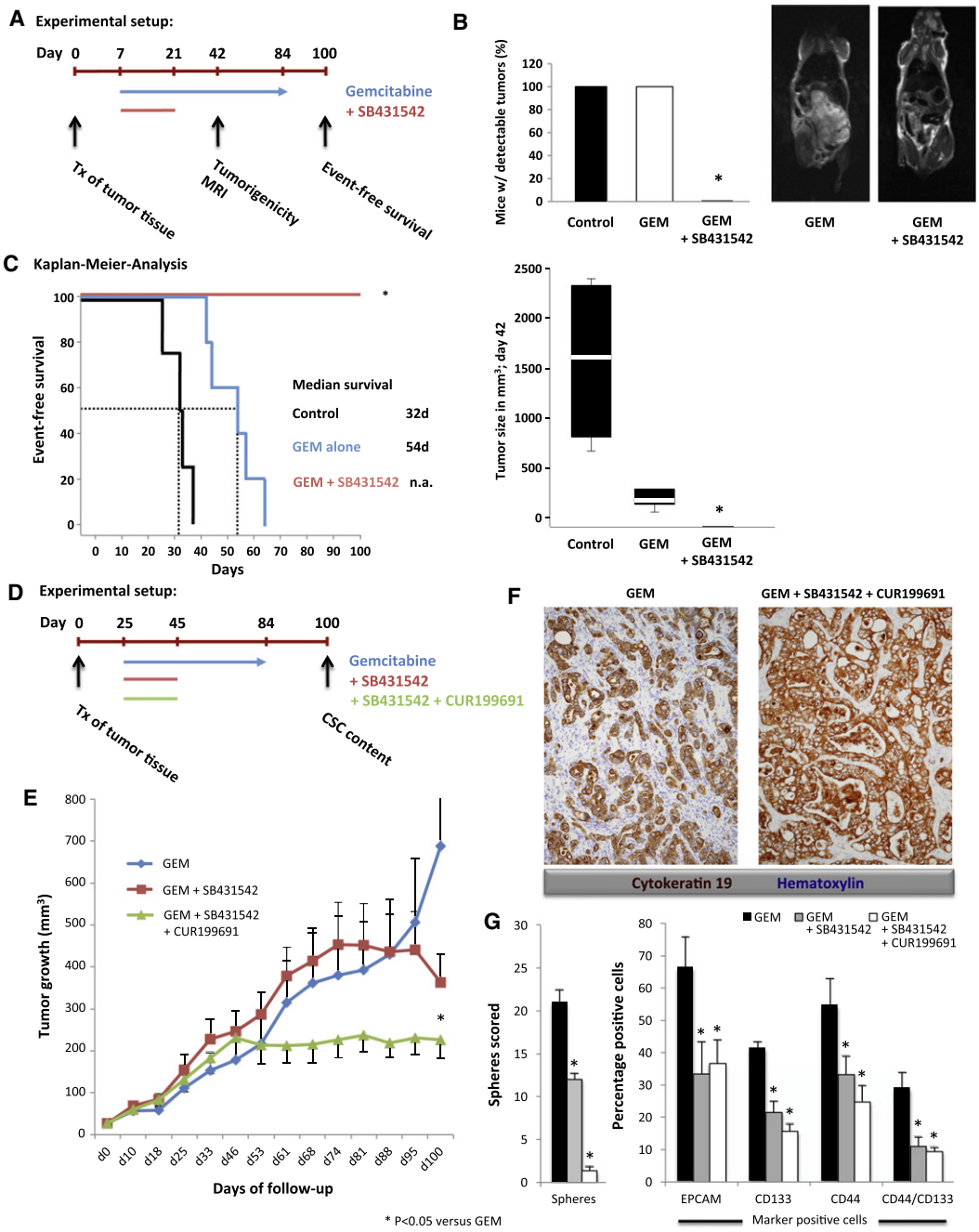

Figure 7. In Vivo Effects of Nodal/Activin Inhibition on Established Pancreatic Cancers

(A) Experimental setup for in vivo experiments using L3.6pl cells.

(B) Tumor take-rate (upper left panel), tumor size (lower panel), and representative MRI pictures (right panel) of treated pancreatic cancers.

(C) Kaplan-Meier analysis depicting cumulative survival of respective treatment groups; data are mean ± SEM, n ≥ 3.

(D) Experimental setup for in vivo experiments using primary human pancreatic cancer tissue.

(E) Tumor growth is depicted for the respective treatment groups. Data are mean ± SEM, n ≥ 3.

(F) Histological evaluation on day 100 using cytokeratin 19 staining for gemcitabine alone (GEM) and triple-treated tumors as indicated.

(G) On day 100, tumors from the different groups were digested and analyzed for their respective sphere formation capacity (left panel) and cell surface marker expression (right panel); data are mean ± SEM, n ≥ 3.

See also Figures S5–S7.

by using recombinant Lefty as the specific endogenous Nodal inhibitor; and third, by genetic knockdown of *Nodal*, *Alk4*, and *Smad4* using shRNA technology. Our findings are in line with earlier observations that have identified other developmental pathways such as mTOR, hedgehog, Notch, and BMP for targeting CSCs (Bar et al., 2007; Li et al., 2007; Mueller et al., 2009;

Piccirillo and Vescovi, 2006), although their targeting may be of limited clinical use for at least some of them due to normal stem-cell-related side effects. Intriguingly, an important feature of the herein described Nodal/Activin pathway is its complete lack of activity in normal pancreas and other adult tissue (Topczewska et al., 2006), spurring the hope for little to no side effects because normal stem cells will most likely be spared.

Nodal and Activin are involved in developmental biology by perpetuating the undifferentiated state of ESCs (Vallier et al., 2005; Xiao et al., 2006). While the expression of Activin and the Nodal coreceptor Cripto-1 have previously been demonstrated in pancreatic cancers (Friess et al., 1994; Kleeff et al., 1998), we here provide evidence that Nodal, the second ligand of the Alk4/7 receptor, is expressed in this malignancy, but not in normal pancreas. Most importantly, Nodal is capable of strongly propagating the tumorigenic CSC subpopulation as demonstrated by its pharmacological inhibition using the extracellular Nodal antagonist Lefty and shRNA technology, whereas Activin was less drastically enriched in pancreatic CSCs and showed limited effects on their self-renewal capacity in some tumors. These data are in line with previous reports showing that Nodal is crucial for tumorigenicity in melanoma and breast cancer cells, with an embryonic microenvironment reducing tumorigenic activity and inducing the expression of epithelial markers by the secretion of Lefty (Postovit et al., 2008; Topczewska et al., 2006).

On the other hand, Activin reportedly contributes to an invasive phenotype in esophageal carcinoma, another epithelial malignancy (Yoshinaga et al., 2004, 2008). In a previous report on the dynamic regulation of the invasive phenotype of breast cancer cell lines, the interconversion from noninvasive epithelial-like $CD44^+CD24^+$ cells to invasive mesenchymal $CD44^+CD24^-$ progeny was also found to be Nodal/Activin dependent (Meyer et al., 2009). Consistently, we now provide evidence that Activin also promotes invasion of pancreatic CSCs as does Nodal. These data have important implications because they indicate that therapeutic strategies should not focus on either Nodal or Activin, but rather focus on Alk4/7 as their common receptor. Indeed, a comprehensive set of experiments proves that targeting this pathway by blocking the Alk4/7 receptor using the small molecule inhibitor SB431542 and shRNA technology has a strong impact on both the $CD133^+$ fraction that is enriched for CSCs and sphere formation capacity.

Next, we identified human PSCs as an important component of the stroma that also strongly expresses Nodal/Activin. Conditioned medium from PSCs promoted self-renewal and invasiveness of pancreatic CSCs. PSCs, which reside in exocrine areas of the pancreas, are myofibroblast-like cells known to be activated upon insult. These cells are analogous to hepatic stellate cells, with which they share 99% identity at the transcriptome level (Omary et al., 2007). PSCs are important mediators in the pancreatic response to injury because they migrate to the damaged location and promote cell proliferation, migration, and assembly (Shimizu, 2008). Therefore, because our data suggest that PSCs may represent an in vivo niche for CSCs, targeting these interactions could be of pivotal importance for the development of more effective therapies for pancreatic cancer. While targeting Alk4/7 as the common receptor for Nodal/Activin should abrogate autocrine and paracrine signaling, directly eliminating this paracrine source for Nodal/Activin may provide additional therapeutic benefits. Intriguingly, this can be achieved by targeting the hedgehog pathway as a crucial signaling component for PSCs (Bailey et al., 2008; Shinozaki et al., 2008), and may account, at least in part, for the striking therapeutic effects generated by the addition of a smoothened inhibitor to our armamentarium for treating primary pancreatic cancer tissue in our studies.

However, translating our findings into the in vivo setting was not only challenged by alternative sources for Nodal/Activin, but also by the fact that the Nodal/Activin small molecule inhibitor SB431542 as a single therapy was not sufficient to irreversibly eliminate the cells' ability to form tumors in vivo. This lack of in vivo translation of the apparently encouraging in vitro effects could be explained by the enhanced plasticity of pancreatic cancer cells. Indeed, after withdrawal of SB431542 and continued culture of the cells, a drastic rebound of the $CD133^+$ population was also observed in vitro, which retrospectively rationalizes the still-preserved in vivo tumorigenicity of the cells. However, the rebound of $CD133^+$ CSCs upon withdrawal was prevented by addition of gemcitabine to the treatment regimen. Further mechanistic studies revealed that SB431542 alone (reversibly) drives CSCs into a more differentiated state, as evidenced by loss of CD133, but cells still retain the ability to revert to the CSC phenotype. Intriguingly, although gemcitabine alone led to a relative enrichment of CSCs, the combination of SB431542 and gemcitabine resulted in their irreversible and complete elimination. Indeed, in vitro combination therapy resulted in complete abrogation of the in vivo tumorigenic potential of the remaining cells.

This chemosensitizing effect of SB431542 should be of great therapeutic value for patients with pancreatic cancer and was therefore further evaluated in vivo. However, testing this treatment regimen in mouse models of pancreatic cancer came with another caveat. Our first in vivo experiments in established pancreatic cancer, which were based on the orthotopic implantation of isolated pancreatic cancer cells, confirmed the in vitro data by illustrating robust therapeutic efficacy and 100% survival at 100 day follow-up for SB431542 plus gemcitabine. Surprisingly, however, when we then moved to a preclinical model using xenografted primary human pancreatic cancer tissue, tumor development remained virtually unaffected by this combination. It is important to note that xenografted pancreatic cancer tissues contain large amounts of stroma whereas implantation of cancer cells regularly lacks this important feature. Tumor-associated stroma does not only provide an additional source for Nodal/Activin as described above, but is also capable of modulating tumor vascularization, which could interfere with drug delivery to cancer (stem) cells. Indeed, impaired drug delivery has already been demonstrated for pancreatic cancer in a recent landmark study using a genetically engineered mouse model (Olive et al., 2009).

Therefore, breaching the "stroma fortress" of pancreatic cancer represents an important challenge for drug delivery in general (Neesse et al., 2010) and CSC-targeted therapies in particular because these cells have been proposed to preferably reside in hypoxic niches (Borovski et al., 2011; Heddleston et al., 2009). Intriguingly, when we coadministered the hedgehog pathway inhibitor CUR199691 (Mueller et al., 2009) to deplete

the stromal compartment together with SB431542, we observed a 10-fold increase in drug delivery into the tumor tissue. The addition of gemcitabine then translated into rapid disease stabilization, and none of the mice required sacrificing during the 100 day study period. Failure to completely eradicate the remaining small tumors can be rationalized by the lack of response of nonproliferating tumor cells to gemcitabine. Most importantly, however, these small lesions no longer contain CSCs; cells isolated from these remnant tumors did not form spheres anymore. In contrast, all mice treated with gemcitabine alone had to be sacrificed within 100 days due to excessive tumor growth. Cells isolated from these tumors bear strong sphere forming capacity. Therefore, our data demonstrate the successful combination of stroma- and CSC-targeting strategies for effectively treating pancreatic cancer in most relevant preclinical models.

Canonical downstream signaling of Alk4/7 is mediated by Smad2/3 as well as the Co-Smad Smad4, which is shared by all TGF-β family members. Importantly, about 50% of patients with pancreatic cancer bear inactivating mutations or deletions of the *Smad4* gene, which could result in dysfunction of the pathway (Schneider and Schmid, 2003). While noncanonical TGF-β family signaling pathways have been described and may account for the enhanced TGF-β1-induced invasiveness of pancreatic CSCs (Zhang, 2009), we found that *Smad4* knockdown in previously Smad4-competent cells resulted in reduced in vivo tumorigenicity, most likely via inhibition of Nodal/Activin signaling, because these cells no longer responded to the Alk4/7 inhibitor SB431542. Therefore, because Smad4 seems indispensable for the Nodal/Activin signaling cascade, tumors carrying functionally relevant *Smad4* mutations or deletions may not respond to a Nodal/Activin-targeting therapy. Importantly, however, not all *Smad4* mutations actually result in dysfunctional Smad4; we have identified several tumors bearing *Smad4* mutations that still demonstrate a functional Smad2/3 cascade, including a subsequent translocation of pSmad2 into the nucleus, and that respond to this triple therapy. Future studies will have to address the question of which patients will most likely respond to this treatment modality and how best to identify them.

EXPERIMENTAL PROCEDURES

Primary Human Pancreatic Cancer Cells

Human pancreatic tumors were obtained with written informed consent from all patients. For in vitro studies, tissue fragments were minced, enzymatically digested with collagenase (Stem Cell Technologies, Vancouver, BC) for 60 min at 37°C (Mueller et al., 2009), and, after centrifugation for 5 min at 1200 rpm, resuspended as pellets and cultured in RPMI, 10% FBS, and 50 units/ml penicillin/streptomycin.

Pancreatic cancer spheres were generated and expanded in DMEM:F12 (Invitrogen, Karlsruhe, Germany) supplemented with B-27 (GIBCO, Karlsruhe, Germany) and bFGF (PeproTech EC, London, UK). Ten thousand cells per milliliter were seeded in ultra-low attachment plates (Corning B.V., Schiphol-Rijk, Netherlands) as described previously (Gallmeier et al., 2011). After 7 days of incubation, spheres were typically >75 μm large with ~97% $CD133^{high}$. For serial passaging, 7-day-old spheres were harvested using 40 μm cell strainers, dissociated to single cells with trypsin, and then regrown for 7 days. Cultures were kept no longer than 4 weeks after recovery from frozen stocks (passage 3–4).

Human Pancreatic Cancer Cell Lines

The human pancreatic cancer cell lines L3.6pl, Panc1, and MiaPaCa2 were maintained as previously described (Hermann et al., 2007).

In Vivo Treatment of Established Pancreatic Cancers

Single-cell suspensions were either orthotopically implanted into the pancreas of female nude mice (Harlan Europe), or 2 mm^3 pieces of primary, in vivo expanded pancreatic cancer tissue were subcutaneously implanted and mice were randomized to the respective treatment groups. Size and weight of the pancreatic tumors were monitored. Gemcitabine was administered twice a week (125 mg/kg i.p.). SB431542 was used at 25 mg/kg, and CUR199691, at 100 mg/kg, both by oral gavages twice daily for 3 weeks.

Cytometry

To identify pancreatic CSCs, the following antibodies were used: anti-CD133/1-APC or PE (Miltenyi, Bergisch-Gladbach, Germany); anti-CXCR4-APC, anti-SSEA-4-FITC, SSEA-1-APC, EpCAM-FITC, and CD44-PE (all from Beckton Dickinson, Heidelberg, Germany); and anti-Alk4, anti-Alk5, and anti-Cripto-1-PE (all from Cell Signaling Technology, Inc.); or appropriate isotype-matched control antibodies. CD133/2-APC (Miltenyi) was used for purity testing after MACS. Propidium iodide, 7-AAD, or DAPI was used for exclusion of dead cells (eBiosciences, San Diego, CA). Samples were analyzed by flow cytometry using a FACS Canto II (BD) and data were analyzed with FlowJo 9.2 software (Ashland, OR).

Immunofluorescence

Primary pancreatic cancer cells and spheres were seeded in 96-well dishes (Corning, NY) and incubated at 37°C for 3 hr. Cells were washed with cold PBS and then fixed with prechilled 4% PFA for 20 min at room temperature. After blocking with 1% bovine serum albumin in PBS-Triton 0.1%, cells were incubated with primary antibodies: Nodal (ab556676; Abcam, Inc.), pSmad2 (3108; Cell Signaling), and EpCAM (BD) overnight at 4°C in the dark. Then cells were washed three times with PBS-Triton 0.1% and incubated with Alexa-Fluor-conjugated secondary antibodies against mouse or rabbit (Invitrogen) at room temperature for 1 hr in the dark. Cells were mounted in Vectashield containing DAPI (Vector Laboratories, Burlingame, CA) and analyzed using an SP5 confocal microscope (Leica, Heidelberg, Germany).

Western Blot Analysis

PVDF membranes containing electrophoretically separated proteins from human primary pancreatic cancer cells and spheres were probed with mouse antibodies against Oct4a (2890), Smad2 (3103; both Cell Signaling Technology), Nanog (ab21624), Nodal (ab556676), GAPDH (ab8245-100; all Abcam), Smad4 (sc-7966; Santa Cruz Biotech), or rabbit antibody against pSmad2 (3108; Cell Signaling), treated with peroxidase-conjugated goat anti-mouse or anti-rabbit Ig secondary antibody (Sigma), and then visualized by enhanced chemiluminescence (Amersham).

Smad2 Phosphorylation Assay

Human primary sphere-derived single cells were grown for 3 hr in DMEM:F12 (GIBCO) without bFGF and B27. Following starvation, cells were incubated for 30 min at 37°C with recombinant human rNodal, Activin, or TGFb1 (R&D) either alone or in the presence of SB431542 (Sigma) or LY2157299 (Axon MedChem, Groningen, Netherlands. Anti-Smad2 and anti-phospho-Smad2 (Ser465/467, Cell Signaling) antibodies were used following the manufacturer's instructions.

RNA Preparation and Real-Time PCR

Total RNAs from human primary pancreatic cancer cells and spheres were extracted with TRIzol kit (Life Technologies Inc.) according to the manufacturer's instructions. One microgram of total RNA was used for cDNA synthesis with SuperScript II reverse transcriptase (Life Technologies Inc.) and random hexamers. Quantitative real-time PCR was performed using SYBR Green PCR master mix (QIAGEN), according to the manufacturer's instructions. The list of utilized primers is depicted in Table S1.

Invasion and Migration Assays

Invasion assays were performed using modified Boyden chambers filled with Matrigel (BioCoat, BD Biosciences, Heidelberg, Germany). Cells were pretreated with SB431542, SB505124, LY2157299, TGF-β receptor II neutralizing antibodies, or recombinant human Lefty for 1 hr. Five hundred microliters of cell suspensions containing 5×10^4 pretreated or untreated cells were added to the Matrigel-coated inserts, and seven hundred and fifty microliters of

serum-free medium with or without recombinant human Nodal, recombinant human Activin, or recombinant human TGF-β1 were added to the lower chamber. The assay chambers were incubated for 22 hr at 37°C. Invaded cells were fixed in 4% PFA and stained with DAPI. The ratio of cells in the lower chamber versus total seeded cells was calculated.

Lentiviral shRNA Delivery

As lentiviral shuttle backbone we used a pLVX shRNA2 plasmid (Clontech). shRNA constructs were generated by hybridization in solution of HPLC-purified paired oligonucleotides with the recessed restriction sites (BamHI and EcoRI) added to the sequence for cloning purposes. As control we used pLVX-shRNA expression vectors encoding a scrambled shRNA sequence with no target (in silico prediction). The shRNA sequences were selected from the RNAi Consortium website (www.broadinstitute.org/rnai/public). The inserts of shRNA were annealed from sense and antisense oligonucleotides with the sequences as provided in Table S2. Lentivirus production and titration were carried out as previously described (Torres et al., 2011) and regularly contained 1×10^7 T.U./ml with a 1:100 T.U./physical particles ratio as quantitated by qPCR. Cells were then transduced with lentiviral stocks diluted to an M.O.I. of 50 in the presence of polybrene (8 μg/ml, Sigma). A6L and 185 cells were seeded at a density of 5×10^4 cells per 24 multiwell plate and allowed to adhere overnight. The next day, cells were infected with the lentivirus for 6 hr. Stably transduced cells were obtained after cell sorting for GFP included in the viral vector (for *Alk4*, *Alk5*, *Nodal*) or using puromycin resistance (*Smad4*). For the transduction with the Nanog promoter reporter, we used a human Nanog-RFP construct with a zeomycin resistance marker for System Biosciences (SBI; Mountain View, CA).

MRI

Mice were analyzed with a 3-Tesla MRI system (Magnetom Tim Trio, Siemens, Erlangen, Germany) using a dedicated small animal coil and T2-weighted scanning.

Statistical Analyses

Results for continuous variables are presented as means ± standard deviation (SD) unless stated otherwise. Treatment groups were compared with the independent samples t test. Pair-wise multiple comparisons were performed with the one-way ANOVA (two-sided) with Bonferroni adjustment. $p < 0.05$ was considered statistically significant. All analyses were performed using SPSS 17.0 (SPSS Inc., Chicago, Illinois).

SUPPLEMENTAL INFORMATION

Supplemental Information for this article includes two tables and seven figures and can be found with this article online at doi:10.1016/j.stem.2011.10.001.

ACKNOWLEDGMENTS

We are indebted to Mercedes Alonso for excellent technical assistance and Francisco X. Real for providing primary tissue samples (both from the Spanish National Cancer Research Centre). This work was supported by the Dr. Mildred Scheel Foundation (108168), the ERC Advanced Investigator Grant (Pa-CSC 233460), the Subdirección General de Evaluación y Fomento de la Investigación, Fondo de Investigación Sanitaria (PS09/02129), and the Programa Nacional de Internacionalización de la I+D, Subprogramma: FCCI 2009 (PLE2009-0105; both Ministerio de Ciencia e Innovación, Spain). E.L. is supported by the Roche Postdoctoral Fellowship Program. Ludwig-Maximilian-University and the Spanish National Cancer Research Centre have filed a patent application for the use of the described treatment modality for epithelial cancer. The authors (E.L., M.T.M., P.C.H., S.H., and C.H.) are inventors of these patents, and may receive royalties from licensees.

Received: February 25, 2011
Revised: September 5, 2011
Accepted: October 3, 2011
Published: November 3, 2011

REFERENCES

Bailey, J.M., Swanson, B.J., Hamada, T., Eggers, J.P., Singh, P.K., Caffery, T., Ouellette, M.M., and Hollingsworth, M.A. (2008). Sonic hedgehog promotes desmoplasia in pancreatic cancer. Clin. Cancer Res. *14*, 5995–6004.

Bar, E.E., Chaudhry, A., Lin, A., Fan, X., Schreck, K., Matsui, W., Piccirillo, S., Vescovi, A.L., DiMeco, F., Olivi, A., and Eberhart, C.G. (2007). Cyclopamine-mediated hedgehog pathway inhibition depletes stem-like cancer cells in glioblastoma. Stem Cells *25*, 2524–2533.

Borovski, T., De Sousa, E., Melo, F., Vermeulen, L., and Medema, J.P. (2011). Cancer Stem Cell Niche: The Place to Be. Cancer Research *71*, 634–639.

Engelmann, K., Shen, H., and Finn, O.J. (2008). MCF7 side population cells with characteristics of cancer stem/progenitor cells express the tumor antigen MUC1. Cancer Res. *68*, 2419–2426.

Friess, H., Yamanaka, Y., Büchler, M., Kobrin, M.S., Tahara, E., and Korc, M. (1994). Cripto, a member of the epidermal growth factor family, is over-expressed in human pancreatic cancer and chronic pancreatitis. Int. J. Cancer *56*, 668–674.

Gallmeier, E., Hermann, P.C., Mueller, M.T., Machado, J.G., Ziesch, A., De Toni, E.N., Palagyi, A., Eisen, C., Ellwart, J.W., Rivera, J., et al. (2011). Inhibition of ATR Function Abrogates the in Vitro and in Vivo Tumorigenicity of Human Colon Cancer Cells Through Depletion of the CD133+ Tumor-Initiating Cell Fraction. Stem Cells *29*, 418–429.

Heddleston, J.M., Li, Z., McLendon, R.E., Hjelmeland, A.B., and Rich, J.N. (2009). The hypoxic microenvironment maintains glioblastoma stem cells and promotes reprogramming towards a cancer stem cell phenotype. Cell Cycle *8*, 3274–3284.

Hendrix, M.J., Seftor, E.A., Seftor, R.E., Kasemeier-Kulesa, J., Kulesa, P.M., and Postovit, L.M. (2007). Reprogramming metastatic tumour cells with embryonic microenvironments. Nat. Rev. Cancer *7*, 246–255.

Hermann, P.C., Huber, S.L., Herrler, T., Aicher, A., Ellwart, J.W., Guba, M., Bruns, C.J., and Heeschen, C. (2007). Distinct populations of cancer stem cells determine tumor growth and metastatic activity in human pancreatic cancer. Cell Stem Cell *1*, 313–323.

Hermann, P.C., Huber, S.L., and Heeschen, C. (2008). Metastatic cancer stem cells: a new target for anti-cancer therapy? Cell Cycle *7*, 188–193.

Jesnowski, R., Fürst, D., Ringel, J., Chen, Y., Schrödel, A., Kleeff, J., Kolb, A., Schareck, W.D., and Löhr, M. (2005). Immortalization of pancreatic stellate cells as an in vitro model of pancreatic fibrosis: deactivation is induced by matrigel and N-acetylcysteine. Lab. Invest. *85*, 1276–1291.

Jones, S., Zhang, X., Parsons, D.W., Lin, J.C., Leary, R.J., Angenendt, P., Mankoo, P., Carter, H., Kamiyama, H., Jimeno, A., et al. (2008). Core signaling pathways in human pancreatic cancers revealed by global genomic analyses. Science *321*, 1801–1806.

Kleeff, J., Ishiwata, T., Friess, H., Büchler, M.W., and Korc, M. (1998). Concomitant over-expression of activin/inhibin beta subunits and their receptors in human pancreatic cancer. Int. J. Cancer *77*, 860–868.

Li, C., Heidt, D.G., Dalerba, P., Burant, C.F., Zhang, L., Adsay, V., Wicha, M., Clarke, M.F., and Simeone, D.M. (2007). Identification of pancreatic cancer stem cells. Cancer Res. *67*, 1030–1037.

Massagué, J. (2008). TGFbeta in Cancer. Cell *134*, 215–230.

Meyer, M.J., Fleming, J.M., Ali, M.A., Pesesky, M.W., Ginsburg, E., and Vonderhaar, B.K. (2009). Dynamic regulation of CD24 and the invasive, CD44posCD24neg phenotype in breast cancer cell lines. Breast Cancer Res. *11*, R82.

Mueller, M.T., Hermann, P.C., Witthauer, J., Rubio-Viqueira, B., Leicht, S.F., Huber, S., Ellwart, J.W., Mustafa, M., Bartenstein, P., D'Haese, J.G., et al. (2009). Combined targeted treatment to eliminate tumorigenic cancer stem cells in human pancreatic cancer. Gastroenterology *137*, 1102–1113.

Neesse, A., Michl, P., Frese, K.K., Feig, C., Cook, N., Jacobetz, M.A., Lolkema, M.P., Buchholz, M., Olive, K.P., Gress, T.M., and Tuveson, D.A. (2010). Stromal biology and therapy in pancreatic cancer. Gut *60*, 861–868.

Ohnishi, N., Miyata, T., Ohnishi, H., Yasuda, H., Tamada, K., Ueda, N., Mashima, H., and Sugano, K. (2003). Activin A is an autocrine activator of rat

pancreatic stellate cells: potential therapeutic role of follistatin for pancreatic fibrosis. Gut *52*, 1487–1493.

Olive, K.P., Jacobetz, M.A., Davidson, C.J., Gopinathan, A., McIntyre, D., Honess, D., Madhu, B., Goldgraben, M.A., Caldwell, M.E., Allard, D., et al. (2009). Inhibition of Hedgehog signaling enhances delivery of chemotherapy in a mouse model of pancreatic cancer. Science *324*, 1457–1461.

Omary, M.B., Lugea, A., Lowe, A.W., and Pandol, S.J. (2007). The pancreatic stellate cell: a star on the rise in pancreatic diseases. J. Clin. Invest. *117*, 50–59.

Piccirillo, S.G., and Vescovi, A.L. (2006). Bone morphogenetic proteins regulate tumorigenicity in human glioblastoma stem cells. Ernst Schering Found. Symp. Proc. *2006*, 59–81.

Postovit, L.M., Margaryan, N.V., Seftor, E.A., Kirschmann, D.A., Lipavsky, A., Wheaton, W.W., Abbott, D.E., Seftor, R.E., and Hendrix, M.J. (2008). Human embryonic stem cell microenvironment suppresses the tumorigenic phenotype of aggressive cancer cells. Proc. Natl. Acad. Sci. USA *105*, 4329–4334.

Rubio-Viqueira, B., Jimeno, A., Cusatis, G., Zhang, X., Iacobuzio-Donahue, C., Karikari, C., Shi, C., Danenberg, K., Danenberg, P.V., Kuramochi, H., et al. (2006). An in vivo platform for translational drug development in pancreatic cancer. Clin. Cancer Res. *12*, 4652–4661.

Scaffidi, P., and Misteli, T. (2011). In vitro generation of human cells with cancer stem cell properties. Nat. Cell Biol. *13*, 1051–1061.

Schneider, G., and Schmid, R.M. (2003). Genetic alterations in pancreatic carcinoma. Mol. Cancer *2*, 15.

Shimizu, K. (2008). Mechanisms of pancreatic fibrosis and applications to the treatment of chronic pancreatitis. J. Gastroenterol. *43*, 823–832.

Shinozaki, S., Ohnishi, H., Hama, K., Kita, H., Yamamoto, H., Osawa, H., Sato, K., Tamada, K., Mashima, H., and Sugano, K. (2008). Indian hedgehog promotes the migration of rat activated pancreatic stellate cells by increasing membrane type-1 matrix metalloproteinase on the plasma membrane. J. Cell. Physiol. *216*, 38–46.

Strizzi, L., Bianco, C., Normanno, N., and Salomon, D. (2005). Cripto-1: a multifunctional modulator during embryogenesis and oncogenesis. Oncogene *24*, 5731–5741.

Topczewska, J.M., Postovit, L.M., Margaryan, N.V., Sam, A., Hess, A.R., Wheaton, W.W., Nickoloff, B.J., Topczewski, J., and Hendrix, M.J. (2006). Embryonic and tumorigenic pathways converge via Nodal signaling: role in melanoma aggressiveness. Nat. Med. *12*, 925–932.

Torres, R., García, A., Payá, M., and Ramirez, J.C. (2011). Non-integrative lentivirus drives high-frequency cre-mediated cassette exchange in human cells. PLoS ONE *6*, e19794.

Vallier, L., Alexander, M., and Pedersen, R.A. (2005). Activin/Nodal and FGF pathways cooperate to maintain pluripotency of human embryonic stem cells. J. Cell Sci. *118*, 4495–4509.

Watabe, T., and Miyazono, K. (2009). Roles of TGF-beta family signaling in stem cell renewal and differentiation. Cell Res. *19*, 103–115.

Xiao, L., Yuan, X., and Sharkis, S.J. (2006). Activin A maintains self-renewal and regulates fibroblast growth factor, Wnt, and bone morphogenic protein pathways in human embryonic stem cells. Stem Cells *24*, 1476–1486.

Yoshinaga, K., Inoue, H., Utsunomiya, T., Sonoda, H., Masuda, T., Mimori, K., Tanaka, Y., and Mori, M. (2004). N-cadherin is regulated by activin A and associated with tumor aggressiveness in esophageal carcinoma. Clin. Cancer Res. *10*, 5702–5707.

Yoshinaga, K., Yamashita, K., Mimori, K., Tanaka, F., Inoue, H., and Mori, M. (2008). Activin a causes cancer cell aggressiveness in esophageal squamous cell carcinoma cells. Ann. Surg. Oncol. *15*, 96–103.

Zhang, Y.E. (2009). Non-Smad pathways in TGF-beta signaling. Cell Res. *19*, 128–139.

Update

Cell Stem Cell
Volume 10, Issue 1, 6 January 2012, Page 104

DOI: https://doi.org/10.1016/j.stem.2011.12.001

Cell Stem Cell
Correction

Nodal/Activin Signaling Drives Self-Renewal and Tumorigenicity of Pancreatic Cancer Stem Cells and Provides a Target for Combined Drug Therapy

Enza Lonardo, Patrick C. Hermann, Maria-Theresa Mueller, Stephan Huber, Anamaria Balic, Irene Miranda-Lorenzo, Sladjana Zagorac, Sonia Alcala, Iker Rodriguez-Arabaolaza, Juan Carlos Ramirez, Raul Torres-Ruíz, Elena Garcia, Manuel Hidaldo, David Álvaro Cebrián, Rainer Heuchel, Matthias Löhr, Frank Berger, Peter Bartenstein, Alexandra Aicher, and Christopher Heeschen*
*Correspondence: christopher.heeschen@cnio.es
DOI 10.1016/j.stem.2011.12.001

(Cell Stem Cell *9*, 433–446, November 4, 2011)
The supplemental information file originally published with this article inadvertently showed Figure S6 in the place of Figure S4. A corrected version has now been posted online in its place. We apologize for any confusion caused.